

Study of the Conformational Structure and Cluster Formation in a Langmuir–Blodgett Film Using Second Harmonic Generation, Second Harmonic Microscopy, and FTIR Spectroscopy

M. S. Johal,* A. N. Parikh, Y. Lee, J. L. Casson, L. Foster, B. I. Swanson, D. W. McBranch, D. Q. Li, and J. M. Robinson

Chemical Science & Technology Division, Los Alamos National Laboratory,
Los Alamos, New Mexico 87545

Received August 20, 1998. In Final Form: November 16, 1998

Nonlinear second harmonic generation (SHG), second harmonic microscopy (SHM), and infrared spectroscopy are used to determine the structural and optical properties of the Langmuir–Blodgett (LB) monolayer assemblies of NLO-active, 4-eicosyloxo-(E)-stilbazolium iodide (4-EOSI) on a glass substrate. The packing characteristics of the pretransferred interfacial films are determined using π -A isotherm measurements. The molecular coverage of the transferred films is determined by ellipsometry. The films formed on both sides of the glass substrate show substantial second harmonic (SH) conversion from p-polarized 1064 nm fundamental excitation. The SHG and FTIR measurements imply that the single LB layer on glass is composed of oriented clusters of 4-EOSI molecules that are laterally discontinuous. Ordered clusters up to 40 μ m in diameter are directly observed using SHM. Subsequent LB transfers using the same 4-EOSI molecule or an amphiphile of comparable chain-length (eicosanoic acid) fill in the unoccupied vacancies in the first layer. The magnitude of the dominant element of the nonlinear susceptibility and the average molecular orientation angle of the chromophore are determined by modeling the characteristic SHG Maker fringes.

Introduction

The Langmuir–Blodgett (LB) technique is a reliable method for preparing well-ordered ultrathin organic films on a variety of solid substrates. In recent years, there has been an increasing interest in the nonlinear optical (NLO) properties of such systems because they are polar-ordered Y-structure (or herringbone) films. For close-packed LB monolayers in particular, this high degree of ordering makes optical nonlinearity an inherent property.^{1–3} To date, the subjects of NLO studies of LB films on solid substrates range from polymer systems^{4,5} and coordination compounds^{6,7} to optical dyes.⁸ In this work, the three techniques of second harmonic generation (SHG), second harmonic microscopy (SHM), and Fourier transform infrared (FT IR) spectroscopy are used to investigate the structural and NLO properties of a new stilbene-based derivative, 4-eicosyloxo-(E)-stilbazolium iodide (4-EOSI) (Figure 1). The donor–acceptor groups in the chromophore and the delocalized π -electrons associated with the stilbene structure make this molecule an attractive candidate for NLO studies.

SHG is an intrinsically surface-specific, second-order optical effect that can yield information on surface

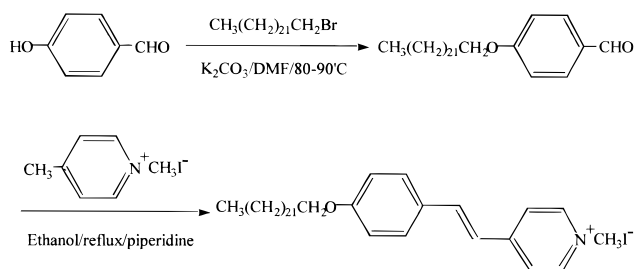


Figure 1. Structure and synthesis of 4-eicosyloxo-(E)-stilbazolium iodide (4-EOSI).

symmetry and order.⁹ SHM is a recently developed microscopic imaging technique based on SHG.^{10–12} In this work, a clear distinction is made between SHG and SHM as surface analytical techniques. In SHG, the second harmonic (SH) signal is measured integrally, yielding interfacial order and symmetry averaged over an illuminated spot. In contrast, SHM reveals the lateral variation in nonlinearities due to *local* symmetry and order. SHM has been used to image several systems, from surface diffusion measurements on semiconductors¹³ to photolithographically patterned self-assembled monolayers.¹² This is the first use of the technique to directly observe clusters in LB films. Langmuir films on the surface of water have previously been observed by Flörscheimer

(1) Decher, G.; Tieke, B.; Bosshard, C.; Gunter, P. *Ferroelectrics* **1989**, *91*, 193.

(2) *New Developments in Construction and Function of Organic Thin Films*; Mobius, D., Miller, R., Eds.; Elsevier: Amsterdam, 1996.

(3) Decher, G.; Tieke, B.; Bosshard, C.; Gunter, P. *J. Am. Chem. Soc. Commun.* **1988**, *14*, 933.

(4) Tang, Q.; Zahir, S. A.; Bosshard, C.; Flörscheimer, M.; Kupfer, M.; Gunter, P. *Thin Solid Films* **1992**, *210*, 195.

(5) Takahashi, T.; Chen, Y. M.; Rahaman, A. K.; Kumar, J.; Tripathy, S. K. *Thin Solid Films* **1992**, *210*, 202.

(6) Gao, L. H.; Wang, K. Z.; Huang, C. H.; Zhou, Y. F.; Li, T. K.; Xu, J. M.; Zhao, X. S.; Xia, X. H. *Thin Solid Films* **1996**, *286*, 237.

(7) Gao, L. H.; Wang, K. Z.; Huang, C. H.; Zhao, X. S.; Xia, X. H.; Xu, J. M.; Li, T. K. *Chem. Lett.* **1995**, *11*, 1049.

(8) Schoondorp, M. A.; Schouten, A. J.; Hulshof, J. B. E.; Feringa, B. L. *Thin Solid Films* **1992**, *210*, 166.

(9) Shen, Y. R. *Principles of Nonlinear Optics*; Wiley: New York, 1984.

(10) Flörscheimer, M.; Bösch, M.; Brillert, Ch.; Wierschem, M.; Fuchs, H. *J. Vac. Sci. Technol., B* **1997**, *15*, 1564.

(11) Flörscheimer, M.; Bösch, M.; Brillert, Ch.; Wierschem, M.; Fuchs, H. *Adv. Mater.* **1997**, *9*, 1061.

(12) Smilowitz, L.; Jia, Q. X.; Yang, X.; Li, D. Q.; McBranch, D.; Buelow, S. J.; Robinson, J. M. *J. Appl. Phys.* **1997**, *81*, 2051.

(13) Allen, C. E.; Ditchfield, R.; Seebauer, E. G. *J. Vac. Sci. Technol., A* **1996**, *14*, 22.

et al., who showed that the lateral structure of an ultrathin organic film could be imaged by SHM.¹⁴

In this work, LB films of 4-EOSI were prepared by the vertical transfer of the preformed, condensed interfacial film phase onto a glass substrate. Prior to LB deposition on glass, the quality of the monomolecular film at the air–water interface was characterized using pressure–area isotherm measurements. The SHG and FTIR data, along with ellipsometric measurements of film thickness, suggest that the single LB layers of 4-EOSI on glass form as discontinuous islands. These islands were resolved using SHM. The vacancies in this single layer can be filled by subsequent LB transfers of either the same film (4-EOSI) or from condensed Langmuir phases of long-chain carboxylic acid molecules.

Experimental Approach

Synthesis of 4-EOSI. 4-EOSI was prepared by first synthesizing the intermediate 4-eicosyloxybenzaldehyde (4-EOBA) from the reaction of 4-hydroxybenzaldehyde and 1-bromoeicosane catalyzed by potassium carbonate in *N,N*-dimethyl formamide (DMF) at 110 °C for 18 h. 4-EOBA was subsequently converted to 4-EOSI by its reaction with 1,4-dimethylpyridinium iodide in ethanol under reflux for 8 h.

4-EOBA. 1-Bromoeicosane (2.95 g, 8.16 mmol) was added to 4-hydroxybenzaldehyde (1.02 g, 8.19 mmol) in DMF (20 mL) and the mixture was heated and maintained at 100 °C. The reaction progress was monitored by noting the disappearance of 4-hydroxybenzaldehyde by thin-layer chromatography (TLC). After completion, the reaction mixture was cooled to room temperature and water (25 mL) was added. The product was extracted twice from ethyl ether (2 × 30 mL). The combined ether extracts were dried over anhydrous sodium sulfate and concentrated under reduced pressure. The crude product was purified by column chromatography. The yield was 3.03 g (92%).

4-EOSI. 1,4-Dimethylpyridinium iodide (1.16 g, 4.93 mmol) and catalytic piperidine were dissolved in 30 mL of ethanol. 4-EOBA (2.01 g, 4.96 mmol) was added to the reaction vessel. The reaction mixture was heated to reflux for 8 h and then cooled to room temperature. The product was crystallized from ethanol followed by recrystallization from a mixture of methylene chloride and ethanol (50:50 vol %). The yield was 2.76 g (91%). The NMR and IR spectra of 4-EOBI and 4-EOSI were consistent with their structures.

Preparation and Cleaning of Si Substrates. Double-sided polished Si(111) substrates (Float Zone Si), 1 mm thick with a 0.25° wedge, were used for the ellipsometry and FTIR spectroscopy measurements. The substrates were thoroughly degreased by ultrasonication in HPLC grade chloroform for ~5 min and oxidized using a combination of chemical (*piranha etch* treatment) and photochemical (UV/ozone oxidation) treatments such that the final step was always photochemical.¹⁵ In the *piranha etch* treatment, the samples were immersed for a period of 5–10 min in a freshly prepared 4:1 v/v mixture of sulfuric acid and hydrogen peroxide at 100–110 °C.¹⁶ The samples were then rinsed with copious amounts of organic-free, deionized water and dried under a stream of nitrogen. The UV/ozone treatment¹⁷ was carried out using a commercial UV/ozone reactor (Boekel Scientific). The samples were exposed to the ozone-generating lamp grid (187–254 nm) for ~10–15 min. Previously used substrates were recycled by first stripping the oxide layer by exposing them to buffered ammonium hydrogen fluoride solutions for 45–60 s followed by forming a pristine oxide layer using the combination of the chemical and photochemical processes described above. Freshly oxidized samples were then utilized for monolayer formation within several minutes of the pretreatment process.

Langmuir Isotherms and LB Depositions. A computer-controlled LB system (NIMA Technologies) with a 600 cm² polytetrafluoroethylene (PTFE) trough and Teflon-coated, moving barriers was used for film deposition. The pressure measurements were performed by the Wilhelmy plate method. The subphase pH was monitored using a pH sensor (EDT Instruments), and the subphase temperature was controlled to within ±0.2 °C using a circulating waterbath. The temperature of the ambient medium (air) was not controlled, but was monitored to be ~20.4 ± 0.4 °C for all measurements reported here. The entire trough apparatus was placed in a closed cabinet to minimize thermal fluctuations, the surface settling of airborne dust particles, and adventitious molecules.

A 1 mg/mL solution of 4-EOSI molecules in HPLC grade chloroform was spread drop-by-drop from a chloroform-cleaned, glass microsyringe to the subphase surface. About 25–100 μL of the 4-EOSI solution was applied to the subphase that consisted of ultrapure, deionized water. The subphase pH was monitored to be ~5.8 during all film preparation and isotherm measurements. The subphase surfaces were agitated using a magnetic stirrer for ~30 min to ensure complete evaporation of the solvent phase. Compression and expansion isotherms were collected in a quasi-static mode when the barriers were brought together at a computer-controlled velocity of 25 cm²/min. Every 25 cm² compression was followed by a 5 s pause in the barrier movement. Monolayer transfers to solid substrates occurred at the surface pressure of 25 mN/m and a pulling rate of 5–10 mm/min. 1, 2, 5, 10, and 15 layers were transferred during the sequential dipping and withdrawing of the substrates in to and out of the subphase medium. All samples were placed in polypropylene containers and stored in a laboratory desiccator before characterization.

Single-Wavelength Ellipsometry. A null-ellipsometer (Rudolph Research) operating at 632.8 nm with a 70° angle of incidence was used with a beam spot of ~2 mm. Measurements¹⁸ were made at three different spots on each sample. The phase shift and amplitude ratio ellipsometric parameters, Δ and Ψ, respectively, were determined from the observed polarizer and analyzer angles. The instrumental precision of the ellipsometric angles was 0.04°. The overall sample-to-sample errors in terms of final calculated film thicknesses were ±2 Å. Ellipsometric measurements were made on the precleaned, bare substrates both prior to and immediately after LB deposition.

The film thickness was determined from the ellipsometric parameters using previously reported procedures.¹⁹ For ultrathin molecular films ($d \ll 1000$ nm), the ellipsometry equations do not allow an independent determination of both the optical function and the thickness of the monolayer films from the Δ and Ψ values. Therefore, the film thickness was determined using independently assigned values of the substrate and film optical or dielectric functions. Substrate optical functions were deduced from the measured ellipsometric angles for the bare samples. The optical constants for the film layer were assumed to be 1.50 + 0i, based on previously measured values for comparable molecules at 632.8 nm.²⁰ An error of 0.05 in the real part of the refractive index would lead to an error of ~1 Å in the final calculated film thickness. This is well within the experimental uncertainties in our measurements.

Infrared Spectroscopy Measurements. Infrared transmission spectra were collected using a Fourier transform spectrometer (Bruker Optics) operating at a 4 cm⁻¹ resolution with an unpolarized focusing beam striking the sample at normal incidence. The beam diameter was apertured to 5 mm. A DTGS detector was used with a scan velocity of 10 kHz. The resulting interferograms from multiple, co-added scans were Fourier transformed with Blackman–Harris three-term apodization and zero filling to increase the point density by a factor of 4, which yielded an effective resolution of less than 0.5 cm⁻¹. Such interpolations do not involve smoothing of the data points and thus allow a more accurate determination of peak positions.²¹

(14) Flörscheimer, M.; Salmen, H.; Bösch, M.; Brillert, Ch.; Wierschem, M.; Fuchs, H. *Adv. Mater.* **1997**, *9*, 1056.

(15) Frantz, P.; Granick, S. *Langmuir* **1992**, *8*, 1176.

(16) *Caution: this mixture reacts violently with organic materials and must be handled with extreme care.*

(17) Vig, J. R. *J. Vac. Sci. Technol.*, **A 1985**, *3*, 1027.

(18) Azzam, R. M. A.; Bashara, N. M. *Ellipsometry and Polarized Light*; North-Holland: Amsterdam, 1977.

(19) McCrackin, F. L.; Passaglia, E.; Stromberg, R. R.; Steinberg, H. *L. J. Res. Natl. Bur. Stand. Sect. A* **1963**, *67*, 363.

(20) (a) den Engelsen, D. *Surf. Sci.* **1976**, *56*, 272; (b) Ducharme, D.; Max, J. J.; Salesse, C.; Leblanc, R. M. *J. Phys. Chem.* **1990**, *94*, 1925.

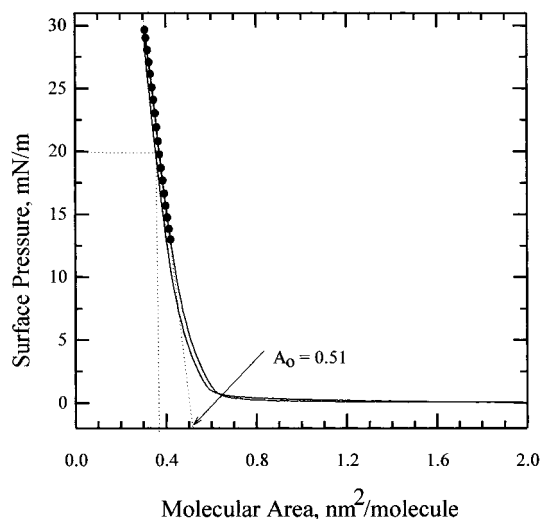


Figure 2. Pressure–area isotherm of 4-EOSI spread on pure water at room temperature.

The spectra of the film samples were referenced against the spectra obtained for the same clean, bare substrate wafers just prior to film deposition. All spectra are reported as $-\log(T/T_0)$, where T and T_0 are the emission power spectra of each sample and reference, respectively.

SHG and SHM Experiments. The SHG measurements were carried out in transmission geometry under nonresonant conditions using p-in and p-out beam polarizations. A mode-locked Nd:YAG laser (Continuum YG501C) provided ~ 25 ps pulses at 10 Hz for fundamental excitation at 1064 nm. The energy density at the sample was ~ 2 mJ/mm². The transmitted SHG signal at 532 nm was measured as a function of the incident angle from normal (0°) to 70° as the sample was rotated in 0.5° steps under computer control.²² The transmitted SHG signal was separated from the fundamental beam using a series of appropriate optical color glass filters and a 532 nm notch filter (Omega). The signal was passed through a polarization analyzer and detected using a photomultiplier tube (Thorn EMI) and gated boxcar integrator (SRS 250). The SH data points were averaged over 100 laser pulses. The SHG signal from a Y-cut quartz crystal was used as a reference.

The same laser system was used for the SHM experiments. The fundamental 1064 nm beam was spatially filtered using a 200 μ m pinhole placed at the focus of a collimating telescope. A liquid-nitrogen-cooled CCD camera (Photometrics) with a 1024×1024 CCD element was focused on the sample microscope slide. This slide was placed at a 70° angle with respect to the laser beam. The 1064 nm beam was 2 mm in diameter with an energy of 4 mJ/pulse. The SH image was acquired using a $4\times$ macroscope mounted on the CCD camera. The pixel size of the CCD element was 24 μ m, giving an overall resolution of 6 μ m. Appropriate optical glass filters ensured that no 1064 nm light reached the CCD camera.

Results and Discussion

Pressure–Area Isotherms. Figure 2 shows the π – A isotherm data for the 4-EOSI molecules spread on a pure water surface. The isotherm trace is characterized by two distinct regions: the initial flat portion of ~ 0 mN/m surface pressure for molecular areas greater than 0.70 nm²/molecule, and a limb of rapidly rising surface pressure for molecular areas of ~ 0.60 – 0.35 nm²/molecule. The assignment of the two observed regimes in terms of simple, molecular phases was made in comparison with the previous reports describing the phase behavior of long-chain surfactant amphiphiles at the air–water interface.²³

In that work, the flat portion of the isotherm was assigned to the G-phase, or gas phase, which was composed essentially of uncorrelated single molecules at the air–water interface. The limb portion was assigned to the LC-phase, or liquid-condensed phase, where the film structure was deduced to be composed of islands of condensed solid-like regions in equilibrium with the G-phase. The present data yields a number of important conclusions regarding the surface amphiphilicity of the 4-EOSI molecules. First, the rapid rise in surface pressure to as high as ~ 30 mN/m in the limb portion of the isotherm trace shows the strong surface amphiphilicity of 4-EOSI molecules at the air–water interface. This allows for the formation of highly oriented single monolayers in condensed phases at the surface of water. Second, the data reveal a noticeable absence of the intermediate LE-phase, or liquid-expanded phase, which is typically observed for surface amphiphiles. This fact, coupled with the presence of a single-limb region characterizing the isotherm, suggests that the compression-induced structural change in 4-EOSI monolayers is the single main-phase transition in 4-EOSI molecules from the initial, two-dimensional G-phase directly to the uniformly condensed solid or LC. This observation implies that the film growth must occur predominantly via island aggregation as opposed to conformational and/or tilting transitions that characterize typical amphiphiles. Finally, the limiting surface area, $A_0 = 0.51$ nm²/molecule, is obtained by extrapolating the limb portion of the isotherm to a zero surface pressure. In comparison, previously reported values for simple, long-chain carboxylic acids are in the range of 0.18 – 0.25 nm²/molecule.²⁴ The larger value obtained for 4-EOSI reflects the dominant role of the bulky headgroup in determining the packing density of the monolayer.

The film thickness of the single-layer LB film on the oxidized silicon substrate was determined by ellipsometry. The thickness on each side of the silicon substrates in three independent preparations fell in a narrow range of $\sim 27 \pm 2$ Å. In comparison to the estimated thickness of ~ 40 Å using simple molecular models, it can be inferred that the surface coverage of transferred monolayers of 4-EOSI on silica substrates is $\sim 60\%$. Given the inaccuracies of the assignments in optical constants of the 4-EOSI molecules, the coverage estimates are accurate within 10%. If we assume the film to be composed of a uniformly tilted 4-EOSI molecules, this estimated coverage would require an average tilt of $\sim 47^\circ$. However, the SHG and FTIR measurements discussed in later sections reveal islanded or discontinuous film structure. As a result, accurate estimations of tilt angles from the ellipsometric data alone cannot be made. One consequence of the nonuniform film morphology is that film structures can have chains or chromophores with significantly lower tilt angles.

FTIR Spectroscopy. Infrared spectroscopy was used to determine the molecular structure of the LB film in terms of chain packing and conformational order. Figures 3a and 4a show representative spectra obtained for single LB layers of 4-EOSI in high (2600 – 3200 cm⁻¹) and low (1100 – 1800 cm⁻¹) frequency regions. Also shown in the bottom panels (Figures 3b and 4b) of the two figures are the respective regions of a typical spectrum of bulk, polycrystalline 4-EOSI solid pressed in a KBr matrix. The high-frequency region of the spectra shows features at ~ 2850 and ~ 2918 cm⁻¹. These features are assigned to

(23) (a) Gaines, G. L., Jr. *Insoluble Monolayers at Liquid–Gas Interfaces*; Wiley-Interscience: New York 1966 and references therein. (b) Knobler, C. M. *Science* **1990**, *249*, 870.

(24) (a) Asgharian, B.; Cadenhead, D. A. *J. Colloid Interface Sci.* **1990**, *134*, 522. (b) Kellner, B. M. J.; Müller-Landau, F.; Cadenhead, D. A. *J. Colloid Interface Sci.* **1978**, *66*, 597.

(21) Buontempo, J. T.; Rice, S. A. *J. Chem. Phys.* **1993**, *98*, 5835.

(22) Maker P. D.; Terhune R. W.; Nisenoff M.; Savage C. M. *Phys. Rev. Lett.* **1962**, *8*, 21.

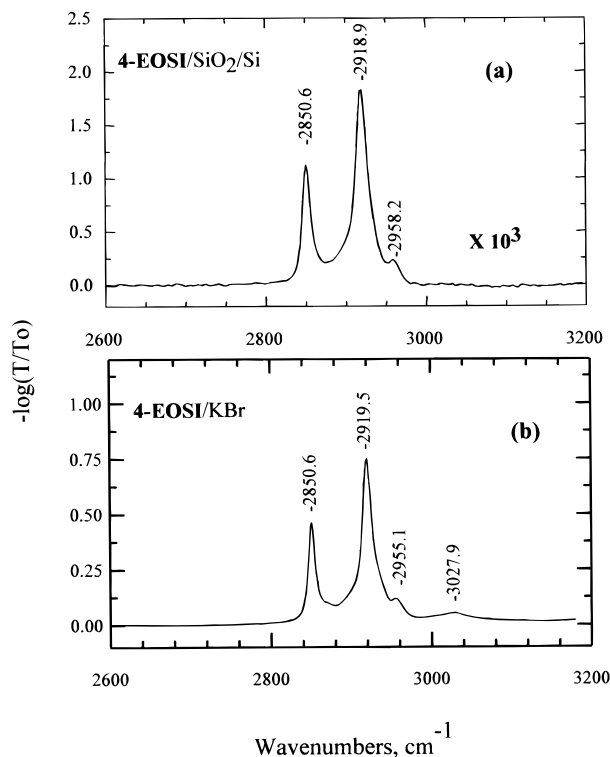


Figure 3. Transmission FTIR spectrum of (a) the single-layer LB film of 4-EOSI and (b) the bulk polycrystalline solid. The spectra were recorded in the high-frequency region (2600–3200 cm^{-1}).

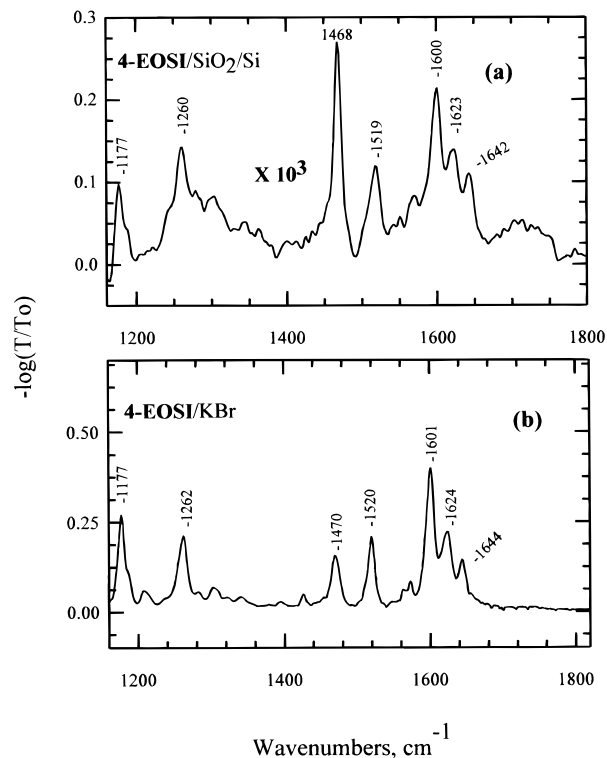


Figure 4. Transmission FTIR spectrum of (a) the single-layer LB film of 4-EOSI and (b) the bulk polycrystalline solid. The spectra were recorded in the low-frequency region (1100–1800 cm^{-1}).

the methylene symmetric (d^+) and antisymmetric (d^-) stretching vibrations, respectively. The weak, but distinct, shoulder observed at $\sim 2958 \text{ cm}^{-1}$ is assigned to the methyl asymmetric stretching mode (r^-). These assignments were

Table 1. Description of Mode Assignments and Comparison of the Peak Positions in cm^{-1} of the Characteristic Bands Observed in the IR Spectra of Bulk, Polycrystalline 4-EOSI Dispersed in a KBr Matrix and Single LB Monolayers of 4-EOSI on a SiO_2/Si Surface (See Text for Details)^a

4-EOSI/KBr	4-EOSI/ SiO_2/Si	mode assignments
3027 (w)		ar. CH str.
2954 (Sh)	2958 (Sh)	CH_3 asym. CH str. (r^-)
2919 (vs)	2918 (vs)	CH_2 antisym. CH str. (d^-)
2850 (vs)	2850 (vs)	CH_2 sym. CH str. (d^+)
1644 (m)	1642 (m)	C=C str.
1624 (m)	1623 (m)	ar. ring str., C=C
1601 (s)	1600 (s)	ar. ring str.
1573 (w), 1562 (w)	1570 (w), 1561 (w)	1,4-C ar. ring str. (quadrant mode)
1519 (m)	1518 (m)	ar. ring str.
1470	1468	CH_2 scissor (δ) + CH_3 deformation
1303, 1341	1303, 1343	CH_2 <i>gauche</i> and kink defect modes
1262	1260	ar. ring in-plane CH bend
1177	1177	C-ring str.

^a Nomenclature: s, strong; m, medium, v, very; w, weak; ar., aromatic; str., stretching; sym., symmetric; asym, asymmetric; antisym, antisymmetric.

made by comparing the spectral assignments to previously reported spectra for *n*-alkanes of comparable chain lengths in bulk, polycrystalline,²⁵ and liquid phases.²⁶ Vibrational modes due to the phenyl ring, olefinic bond, and the aliphatic chain portions of the molecule give rise to many features in the lower frequency region of the spectrum (Figure 4a). Table 1 summarizes the detailed assignment of these peaks to characteristic vibrational modes based on previously reported assignments for comparable solids.²⁷ A comparison of the spectra in the bulk (Figures 3b and 4b) and in the monolayer state (Figures 3a and 4a) reveals that all the dominant spectral features characterizing the bulk, polycrystalline phase of 4-EOSI molecules are present in the monolayer spectra. The similarity in the two spectra shows that, even with a lower packing density, the LB transfer at a solid surface from the condensed monolayer state did not perturb the essential inter- and intramolecular interactions of the 4-EOSI molecules to any noticeable extent. Furthermore, the series of peaks due to the aromatic ring modes in the monolayer spectrum also appear at frequencies comparable to those found in the bulk state (with a marginal red shift of ~ 1 – 2 cm^{-1}). In addition this shows that, despite the close vicinity, the phenyl rings do not participate in any significant π -interaction with the SiO_2/Si interface.

The precise frequencies of the vibrational modes reveal important structural information on the chain region of the monolayer film. The exact location of the d^+ and d^- modes is an important diagnostic marker in determining the chain-conformational order.²⁶ In solid crystalline phases, the symmetric methylene stretches (d^+) of alkyl chains occur between 2848 and 2850 cm^{-1} and the antisymmetric stretches (d^-) are observed between 2916 and 2918 cm^{-1} . However, for a conformationally disordered liquid phase, absorptions due to d^+ and d^- modes occur at distinctly higher ranges of 2856–2858 and 2924–2928

(25) (a) Snyder, R. G.; Schachtschneider, J. H. *Spectrochim. Acta* **1963**, *19*, 85. (b) Snyder, R. G.; Hsu, S. L.; Krimm, S. *Spectrochim. Acta, Part A* **1978**, *34*, 395.

(26) Snyder, R. G.; Strauss, H. L.; Elliger, C. A. *J. Phys. Chem.* **1982**, *86*, 5145.

(27) (a) Bellamy, L. J. *The Infrared Spectra of Complex Molecules*; Chapman and Hall: London, 1975; p 374. (b) Saperstein, D. D.; Rabolt, J. F.; Hoover, J. M.; Stroeve, P. *ACS Symp. Ser.* **1992**, *493*, 104. (c) Stroeve, P.; Saperstein, D. D.; Rabolt, J. F. *J. Chem. Phys.* **1990**, *92*, 6958.

cm^{-1} , respectively. The observed frequencies of 2850.6 and 2918 cm^{-1} in the LB film spectrum are clearly consistent with those characterizing a solid crystalline phase. This suggests the presence of essentially all-*trans* ordered chains in a dense, molecular environment comparable to that of crystalline solids. Further, the series of weak peaks evident in the 1150–1300 cm^{-1} region are thought to represent the vestiges from the coupled, wag-twist, progression bands characteristic of all-*trans* ordered chains. However, the peaks observed are not well-resolved in either the bulk or the monolayer spectra, presumably due to overlapping contributions from a very strong and broad absorption centered at 1277 cm^{-1} . The all-*trans* order is not entirely defect-free in the aliphatic chains but is marked by the presence of isolated defects. This fact is evident in the weak, but reproducible peaks observed at 1303 and 1341 cm^{-1} . These peaks have been previously demonstrated²⁸ to imply the presence of isolated chain-kink (*tg'tg't*) and end-*gauche* (*tg*) defects in the polymethylene chains. The occurrence of the defect peaks assigned above in *both* the monolayer and the bulk polycrystalline spectra further suggests that the isolated chain disorder is an intrinsic constraint of the structure of the molecule rather than the consequence of the film formation protocol. The isolated *gauche* defects evident here are known to not prevent the dense packing of the chains,²⁸ but only to marginally perturb the lateral packing of the molecules. Evidence in support of expanded chain-chain distance is found in the singlet at 1467 cm^{-1} assigned to methylene scissoring. The appearance of the single band for the scissoring mode directly suggests the absence of factor-group splitting. Consequently, the packing of the unit cell in the hydrocarbon phase is triclinic or hexagonal.²⁹ Additionally, the observed full-width, half-maximum of 13–14 cm^{-1} is between the values of 8–10 cm^{-1} reported for the dense, crystalline packing of all-*trans* hydrocarbon chains and the values of 18–25 cm^{-1} for disordered alkyl chains.³⁰ This kind of chain packing has been observed before in rotator and symmetrical hexagonal phases that have an expanded lattice. One well-known example is the crystalline 1-dodecanol monolayer at both the air-water and solid-water interface.^{31,32} These phases are known to be composed of a single type of chain in the unit cell undergoing hindered rotational or twisting motions about their long axis.³³

A quantitative analysis of the FTIR data yields further information regarding the overall orientation of hydrocarbon chains. The details of the explicit procedures used for such comparisons have been previously published.³⁴ The approach involves a comparison of the experimental spectral intensities with those calculated by predicting the spectral response for a monolayer quantity of randomly distributed bulk crystallites at the substrate surface. The spectra of the bulk crystallites are first transformed into the intrinsic optical response functions using the Beers-Lambert law and Kramers-Kronig transformation. These values are then used to calculate the spectrum of the

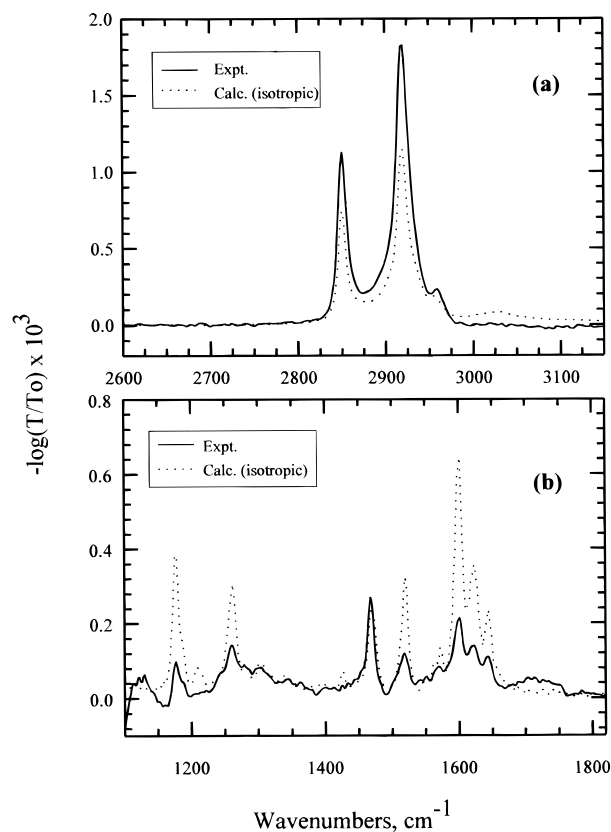


Figure 5. A comparison of the experimental and calculated spectra of the 4-EOSI monolayer. The theoretical basis of the calculated spectrum is discussed in the text.

monolayer quantity³⁵ of randomly oriented crystallites at the SiO_2/Si surface using classical electromagnetic theory.³⁴ The discrepancies in the observed and calculated spectral intensities can then be explained in terms of the orientational differences between the dipolar orientation for the randomly organized, polycrystalline reference state and the LB monolayer state. In order for the above method to be meaningful, it is critical that the reference state used closely approximates the inter- and intramolecular interactions that affect the optical properties. This can be seen in the bulk and monolayer spectra where there is a close correspondence in the peak positions.

A comparison of the experimental and calculated spectra in Figure 5 shows that the predicted intensities for the chain modes in the high-frequency region are strikingly *lower*. However, the calculated positions of the headgroup modes in the lower frequency region are significantly *higher* than the experimentally observed ones. These discrepancies clearly establish that the 4-EOSI in the LB films are not packed in a laterally random organization, but must be arranged in a certain preferred orientation. Explicit simulation of the spectra in terms of precise tilt angles using the present data was determined inconclusive because of the discontinuous, islanded morphology of the film and was not pursued any further. Polarization-dependent spectra measurements for the normal incidence geometry were also not done because identical spectra would have been obtained because of the degeneracy of the polarization states. However, off-normal incidence polarized measurements, in principle, could provide useful data for the estimation of molecular or dipolar tilts in the 4-EOSI films, but were not performed because of the large

(28) Maroncelli, M. A.; Qi, S. P.; Strauss, H. L.; Snyder, R. G. *J. Am. Chem. Soc.* **1982**, *104*, 6237.

(29) Snyder, R. G. *J. Mol. Spectrosc.* **1961**, *7*, 1161.

(30) (a) Cameron, D. G.; Casal, H. L.; Mantsch, H. H.; Boulanger, Y.; Smith, I. C. P. *Biophys. J.* **1981**, *35*, 1 (b) Casal, H. L.; Mantsch, H. H.; Cameron, D. G.; Snyder, R. G. *J. Chem. Phys.* **1982**, *77*, 2825.

(31) Braun, R.; Casson, B. D.; Bain, C. D. *Chem. Phys. Lett.* **1995**, *245*, 326.

(32) Johal, M. S.; Usadi, E. W.; Davies, P. B. *J. Chem. Soc., Faraday Trans.* **1996**, *92*, 573.

(33) Chapman, D. *Trans. Faraday Soc.* **1965**, *61*, 2656.

(34) (a) Nuzzo, R. G.; Dubois, L. H.; Allara, D. L. *J. Am. Chem. Soc.* **1990**, *112*, 558. (b) Parikh, A. N.; Allara, D. L. *J. Chem. Phys.* **1992**, *96*, 927.

(35) The thickness for the bulk crystallites equal to the ellipsometrically determined thickness of the 4-EOSI LB layers was used.

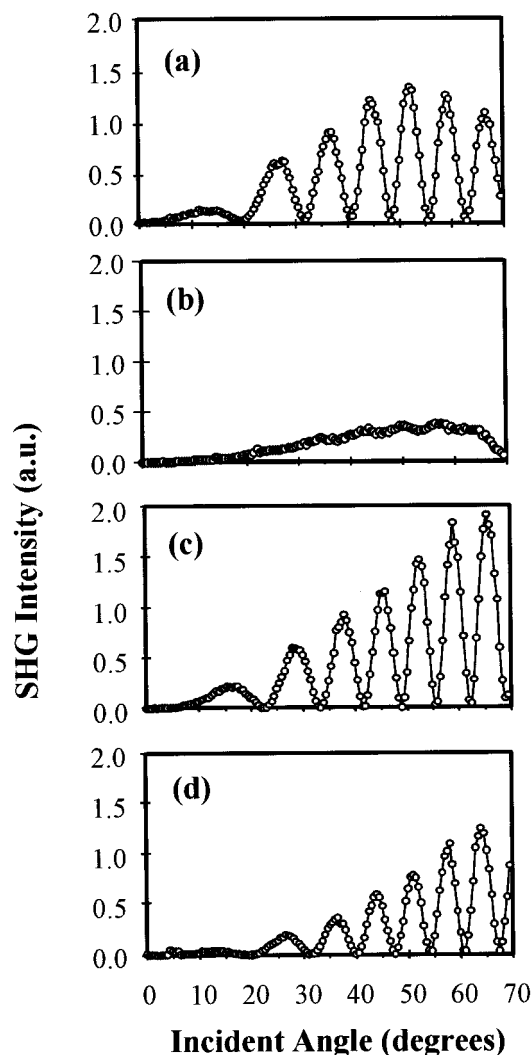


Figure 6. p-in and p-out-polarized SHG data of 4-EOSI LB films as a function of the incident angle of the fundamental beam. The films were assembled on both sides of the glass substrate. The data shown correspond to (a) a single deposition, (b) a single deposition with the film removed from one side of the glass substrate, (c) two depositions, and (d) a single deposition followed by a deposition of eicosanoic acid, followed by a second deposition of 4-EOSI molecules.

uncertainties involved in accurately modeling islanded structures of nonuniform and randomly dispersed clusters. However, we note that the higher predicted intensities of d-modes indicate that the two dipoles interact more strongly with the E-field than they would in their isotropic state. The latter state is equivalent to the collectively tilted state with a molecular tilt of 54.7°. By taking into account the transition dipole moment direction of d-modes, the geometry of the experiments, and higher intensities of the d-modes, we infer that the 4-EOSI molecules must be aligned at an average angle much below 54.7°. Similarly, the directions of the transition moments for the ring quadrant modes in the 1500–1700 cm⁻¹ region along the 1,4-ring axis coupled with the observed lower intensities consistently implies that the axis of the phenyl rings must also make a significantly lower angle than that of the isotropic equivalent.

Second Harmonic Generation. Figure 6a shows the transmitted p-polarized SH intensity from the LB films with layers assembled on both sides of the glass substrate for p-polarized incident excitation. Two major features are observed in the data: the increase in the SH signal

at high angles of incidence and prominent interference fringes. These fringes arise from the interaction of the SH waves from the monolayer on both sides of the substrate as it is rotated.^{36,37} This is confirmed by stripping the film from one side of the glass substrate (using methanol, acetone, and water) and observing that the relative SHG signal decreases and the prominent Maker fringes disappear (Figure 6b). However, very weak fringing is still observed. This is thought to arise from the interaction of the SH waves from the monolayer and the opposite surface of the bare glass substrate.

The lack of azimuthal orientation dependence in the SH signal indicates that the film possesses uniaxial symmetry about the surface normal.³⁸ Thus, only two independent tensor elements (χ_{zzz} and $\chi_{zxx} = \chi_{zyy}$) of the second-order nonlinear susceptibility are nonzero. For p-polarized light at an angle of incidence θ , the p-polarized SHG intensity from the film (I_{pp}) is related to the SHG intensity from the quartz reference (I_{quartz}) by³⁹

$$I_{pp}^{2\omega} = C(\theta) | (2\chi_{xxz} + \chi_{zxx}) \cos^2 \theta_f + \chi_{zzz} \sin^2 \theta_f |^2$$

where

$$C(\theta) = \left[\frac{\pi}{2} \frac{l_f}{I_{\text{quartz}}} \right]^2 \left[\frac{n_{\text{quartz}}}{n_f} \right]^3 \frac{I_{\text{quartz}}^{2\omega}}{|\chi_{xxx}|^2} \times \frac{[T_p^{a-f}(\theta)]^2 T_p^{f-s}(\theta) T_p^{s-a}(\theta) \frac{\sin^2 \theta_f \cos \theta}{\cos^3 \theta_f}}$$

θ_f and θ_s are the angles of refraction in the film and the substrate, respectively, l_f is the film thickness per LB layer, I_{quartz} is the coherence length of the quartz, n_{quartz} and n_f are the refractive indices of the quartz and the film, respectively, and χ_{quartz} is the nonlinear coefficient of quartz when both the fundamental and SH are polarized along the quartz x -axis (i.e., χ_{xxx}). The superscripts a, f, and s in the p-polarized transmissivity, T_p , refer to the air, film, and substrate, respectively. A fit was performed to the data in Figure 6a using the theoretical model based on the above expression as described by Katz et al.³⁹ This involves referencing the χ_{xxx} tensor component of quartz using the SH response from a Y-cut quartz crystal under the same experimental conditions. From the ellipsometric thickness data and the modeled SHG data, the magnitude of the nonlinear coefficient, d_{33} , is 270 pm/V and the average angle of the chromophore is approximately 28° with respect to the surface normal.

The magnitude of the nonlinear coefficient for this single LB film is surprisingly large compared to similar molecules² and reflects the very high degree of polar ordering in the film. The relatively large nonlinear response can also be attributed to the polarizable and delocalized π -electrons associated with the polar-ordered stilbene structure that contains donor–acceptor groups. For comparison, Li et al.³⁸ studied the NLO-active properties of a *p*-bis(3-hydroxypropyl)amino stilbazolium monolayer and found a $d_{33} = 700 \times 10^{-9}$ esu ($d_{33} = 293$ pm/V), which they attributed to the donor–acceptor groups on the NLO-active chromophore. Chromophores which lack such

(36) Li, D. Q.; Swanson, B. I.; Robinson, J. M.; Hoffbauer, M. A. *J. Am. Chem. Soc.* **1993**, *115*, 6975.

(37) Li, D.; Swanson, B. I.; Robinson, J. M.; Hoffbauer, M. A. *Nonlinear Opt. III* **1992**, 1626, 424.

(38) Li, D. Q.; Ratner, M. A.; Marks, T. J.; Zhang, C. H.; Yang, J.; Wong, G. K. *J. Am. Chem. Soc.* **1990**, *112*, 7389.

(39) Katz, H. E.; Scheller, G.; Putvinski, T. M.; Schilling, M. L.; Wilson, W. L.; Chidsey, C. E. D. *Science* **1991**, *250*, 1485.

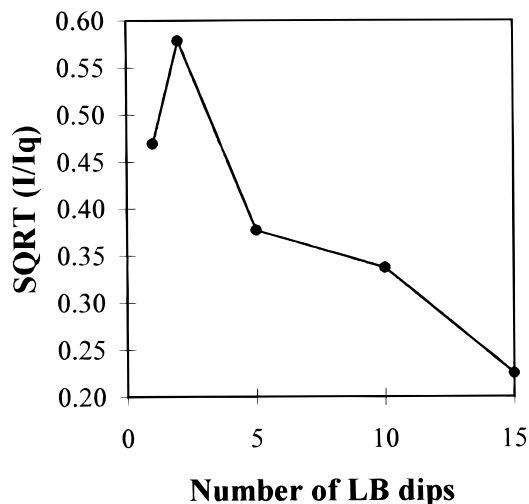


Figure 7. The square root of the maximum SH signal (I_{\max}) normalized to the quartz reference (I_{quartz}) in each case at exactly the same angle of incidence as a function of depositions in the LB trough.

groups yield much lower d_{33} values; for example, the dye multilayer studies by Katz et al.³⁹ show a $d_{33} = 25 \times 10^{-9}$ esu (10.5 pm/V).

Figure 6a represents the SH response from a single LB layer deposited on both sides of the solid substrate. After forming a single layer of 4-EOSI molecules on the substrate, the same substrate was dipped in the LB trough for a second transfer of 4-EOSI molecules. The second-transfer data is shown in Figure 6c. If a complete bilayer was generated after the second transfer, then the SH waves would have opposite phases from each layer, resulting in complete cancellation of the net SH signal. Similarly, all *even*-numbered LB layers would yield no SH signal, while *odd*-numbered layers would generate SH light. However, the SH signal *increases* significantly in going from a single-transfer to double-transfer film. An increase in signal would be expected if the total coverage and packing density of the first layer increased as a result of a second dip. This observation shows that the first transfer results in submonolayer coverage. A subsequent dip in the LB trough simply saturates the first monolayer with the possible formation of a fractional second layer. This would account for the increase in the SH signal observed in Figure 3c.

A third sample was prepared by transferring eicosanoic acid molecules onto the initial 4-EOSI submonolayer. A second transfer of 4-EOSI followed. Figure 6d shows the SHG data obtained from this three-transfer sample. On the basis of the previous conclusion regarding coverage of the first monolayer, the transfer of eicosanoic acid molecules simply completes the undersaturated first layer via strong electrostatic headgroup interactions and hydrophobic chain interactions. The final transfer of 4-EOSI molecules completes the second layer and forms a possible fractional third submonolayer (much like the first submonolayer generated by a single deposition). Partial cancellation of the SH signal from the two layers accounts for the reduction in the SH signal compared to Figure 6c.

Further 5, 10, and 15 LB transfers on the glass substrate were also analyzed. Figure 7 shows the ratio of the square root of the maximum SH signal (I_{\max}) and the quartz reference (I_{quartz}) at exactly the same angle of incidence as a function of dips in the LB trough. The graph shows that the relative SH signal decreases with an increasing number of transfers. Since, as before, a full saturated monolayer is not transferred, all even-numbered transfers

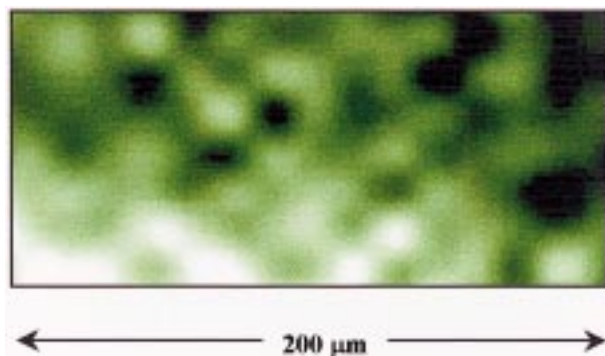


Figure 8. A magnified SHM image of the single-layer LB film assembled on a glass substrate. The resolution of the microscope used to obtain the image was $6 \mu\text{m}$.

still show a SH signal. The decrease in the SH signal probably arises from an increasingly disordered film formed with each subsequent transfer.

Second Harmonic Microscopy. Figure 8 shows the SHM image of the single-layer LB film assembled on a glass substrate. The image clearly shows patches of light and dark regions. The light areas are where SH light has been generated from the LB film and regions of black represent no SHG. A Y-cut quartz sample placed before the spatial filter showed an SH image with no distinct features across the magnified $200 \mu\text{m}$ area when a blank uncoated glass substrate was placed at the focus of the camera. This also confirmed the uniformity of the beam across this area. The intensity of the light regions in the LB film are similar to the SH light generated by the quartz. This was deliberately done for comparison by using much longer exposure times for the LB films. A 45-min exposure time with no microscope slide present at the focus showed that no 1064 nm light reached the CCD camera. The light areas from the LB film are randomly spread to cover about 60% of the observed area and range from 20 to $40 \mu\text{m}$ in diameter. Given the estimated 60% coverage from ellipsometric measurements, the black regions in the SHM image most likely reflects vacancies rather than isotropic phases of 4-EOSI molecules. The SHM image of the LB film is consistent with the formation of relatively large domains ($20\text{--}40 \mu\text{m}$) of well-ordered, but laterally discontinuous, molecules.

Summary

The FTIR spectra reveal that the 4-EOSI films at the SiO_2/Si surface are composed of highly ordered, all-*trans* alkyl chains packed in a crystalline-like molecular environment. The average chain as well as the phenyl rings assume a collective, preferred orientation well-below the isotropic equivalent of a 54.7° tilt of the chain and ring molecular axes. The lateral interactions between the alkyl chains appear to be weaker than those for polycrystalline *n*-alkanes, resulting in an expanded single-chain unit cell equivalent to the rotator phase in *n*-alkanes.

The high degree of order is consistent with the large magnitude of the nonlinear coefficient. The SHG data show that the first LB deposition results in submonolayer coverage, with the second transfer increasing the coverage and packing density of the first monolayer as reflected by an increase in the SHG signal. With a coverage estimated to be 60% from ellipsometric thickness and the FTIR spectra suggesting a well-ordered film, the 4-EOSI molecules must be adsorbed as solid-like island aggregates. Their existence is confirmed by the observation of bright regions ($20\text{--}40 \mu\text{m}$ diameter) in the SHM image. Since

during film formation very slow withdrawal rates were used, kinetics of transfer are unlikely the cause of the low coverage and island formation. More likely, the monolayer relaxes quickly to a more stable structure after the transfer. LB films are known to be metastable and often revert to more stable structures.⁴⁰ The close packing of the alkyl chains and island formation is presumably driven by van der Waals interactions between the hydrophobic C₂₃ tail groups of the 4-EOSI molecules, along with ion-dipole attractions between the stilbazolium headgroups.

This work strongly supports the formation of conformationally well-ordered clusters of 4-EOSI molecules on glass, with subsequent LB layers saturating the first layer and depositing symmetrically. In similar azobenzene systems studied by Schoondorp et al. where a full bilayer (Y-type) is formed, there is complete cancellation of the SHG signal.⁴⁰ This is in contrast to what others have observed in very similar systems where Z-type structures (head-to-tail assembly) have been reported.^{41,42} In Z-type films, which lack a center of inversion, an increase in SHG light would be expected with an increasing number of LB layers. This work clearly shows that Z-type structures are not formed in LB films of 4-EOSI, since a reduction in the SHG signal is observed with an increasing number of LB transfers. It should also be noted that Schoondorp et al. have studied well-ordered domains in LB crystallites of azobenzene and amylose acetate mixtures.⁴³ They saw a large increase in the SHG signal with an increasing number of layers, but only when the sample was annealed.

(40) Schoondorp, M. A.; Schouten, A. J.; Hulshof, J. B. E.; Feringa, B. L. *Langmuir* **1993**, *9*, 1323.

(41) Hayden, L. M.; Kowel, S. T.; Srinivasan, M. P. *Opt. Commun.* **1987**, *61*, 351.

(42) Hayden, L. M.; Anderson, B. L.; Lam, J. Y. S.; Higgins, B. G.; Stroeve, P.; Kowel, S. T. *Thin Solid Films* **1988**, *160*, 379.

The SHG enhancement was attributed to the formation of H-aggregates, which may also occur in 4-EOSI films.

Conclusions

The SHG results suggest that the LB deposition of 4-EOSI results in submonolayer coverage. This is confirmed by the estimated 60% coverage from the ellipsometric thickness measurement. The relatively large magnitude of d_{33} and the orientation angle of the chromophore show that the film is well-ordered. The FTIR data show that the single-layer LB film is solid-like with nearly all-*trans* alkyl chains. The low coverage and conformationally ordered solid-like nature of the film strongly suggests that it forms well-ordered island aggregates on the surface of the glass substrate. These islands were directly observed in the SHM image of the submonolayer LB film. The close-packed island formation is probably driven by the strong hydrophobic interaction between the C₂₃ alkyl chains of the 4-EOSI molecules, along with headgroup ion-dipole interactions. The SHG data also show that subsequent LB transfers lead to coadsorption, with the film disorder increasing with the number of LB depositions.

Acknowledgment. This work was supported by Los Alamos National Laboratory Directed Research and Development, under the auspices of the U.S. Department of Energy.

LA981072V

(43) Schoondorp, M. A.; Schouten, A. J.; Hulshof, J. B. E.; Schudde, E. P.; Feringa, B. L. *Recl. Trav. Chim. Pays-Bas* **1994**, *113* 250.